

Numerical Prediction of a KCS Ship Motion and Response under Focused Waves

Zhihao Wang, Jianhua Wang*, Decheng Wan

Computational Marine Hydrodynamics Lab (CMHL), School of Naval Architecture, Ocean and Civil Engineering,
Shanghai Jiao Tong University, Shanghai, China

*Corresponding Author

ABSTRACT

Focused waves are an extreme type of irregular waves, which can be much higher in wave height than the surrounding waves, posing a serious threat to the safety of marine structures. In this paper, a method based on overset mesh using SUGGAR++ and waves2Foam for generating waves is constructed and numerical simulations of the motion and response of a KCS ship in focused waves are performed. The solver uses naoe-FOAM-SJTU developed within the group. The wave building is performed by a third party software, waves2Foam. The focused wave is generated based on JONSWAP spectra and using new wave model. Changes in bow pressure are more sensitive to changes in wave period. Shorter wave period brings steeper wave lift, which increases the bow pressure.

KEY WORDS: Focused wave; naoe-FOAM-SJTU; overset mesh; slamming.

INTRODUCTION

Focused waves are an extreme type of irregular waves, which can be much higher in wave height than the surrounding waves, posing a serious threat to the safety of marine structures. Studies have found that the acceleration of the ship under the action of focused waves is too large, and the nonlinear motion response amplitude of the hull can reach more than 1.5 times that under normal random waves. In this paper, the ship motion response and thumping load characteristics are investigated for extreme sea conditions. Based on the JONSWAP wind and wave spectra, focused waves focused at different locations on the ship's hull are generated by linear wave superposition, and the ship's motion and thumping under the focused waves are simulated. The effects of different focusing positions on the bang load are analyzed. Stansberg and Karlsen indicated that serious green water event usually occurs in the condition of focused waves, which the huge wave height of focused waves can make a great impact on the ship. Fonseca analyzed the influence of the wave height, wavelength, and waveform of the focused waves on the structural loads, and the results showed that the size of the structure load was related to the maximum wave height of the focused waves and the appearance position of the focused waves. Zhuang et al. focus on the numerical simulation of the interaction of a focused wave with a moving

cylinder. The article employs a higher-order spectrum (HOS) method to generate the focused wave field, combined with a self-developed CFD solver, naoe-FOAM-SJTU (equipped with overlapping mesh technique), to capture the viscous effects around the moving cylinder. Chen et al. explore the complex nonlinear interaction phenomena of focused waves with a finite number of protruding water surface cylinders through high-fidelity numerical simulations to reveal the mechanism of wave scattering. Liu et al. simulate the interaction of a focused wave with a buoy using the computational fluid dynamics (CFD) solver naoe-FOAM-SJTU. The motion response of the wave to the buoy is discussed in the paper. Tromans, Anaturk and Hagemeyer presents a new large ocean wave kinematic model intended to be used as a design wave for offshore structures. The model provides a more accurate representation of the largest waves in a given sea state by taking into account the statistical properties of the peaks and troughs. Specifically, the model reformulates the equations describing wave behavior with deterministic amplitudes and phases, focusing on the occurrence of wave crests under conditional probability statistics. It emphasizes that the surface elevation becomes more deterministic as the height of the wave crest increases, which has significant implications for the loads experienced by offshore structures. In free-surface fluid simulations based on the finite volume method, wave reflections at the boundary of the computational domain can cause significant errors in the results. In order to minimize these reflections, an "implicit relaxation zone" technique can be used, provided that the case-dependent parameters of the relaxation zone are optimized. An analytical method to optimize these parameters was proposed by Perić et al. and their predictions were compared with the results of two-dimensional flow simulations with different depths, wave steepness, flow solvers, and relaxation functions. Comparisons are also made with the results of three-dimensional flow simulations of a strong wave-reflecting object in the presence of nonlinear free surface waves.

NUMERICAL METHOD

Ship Motion

The six-degree-of-freedom module in the naoe-FOAM-SJTU solver is used to calculate the ship's motion in waves. The six-degree-of-freedom divides the motion of the object into three translational motions of surge,

sway and heave and three rotational motions of roll, pitch and yaw. In order to solve these motions, the geodetic coordinate system and the hull coordinate system are established. The position of the geodetic coordinate system is fixed, the hull coordinate system is always fixed on the hull, and its coordinate origin is generally located at the center of gravity. In order to facilitate the understanding of the ship's motion process, the X axis of the coordinate system is generally arranged along the longitudinal direction of the ship, the Y axis is arranged along the width direction of the ship, and the Z axis is arranged along the draft direction. When the ship is in a positive floating state, the geodetic coordinate system is consistent with the positive direction of each coordinate axis of the hull coordinate system.

The movement process of the ship under the geodetic coordinate system is the movement process of the hull coordinate system relative to the geodetic coordinate system, and the displacement of the ship under the geodetic coordinate system can be expressed as:

$$\boldsymbol{\eta} = (\boldsymbol{\eta}_1, \boldsymbol{\eta}_2) = (x, y, z, \phi, \theta, \psi) \quad (1)$$

Among them, the six parameters represent the linear displacement of the ship along the X, Y, and Z axes (surge, sway, heave), and the angular displacement around the X, Y, and Z axes (roll, pitch, yaw). The three linear velocities and the three angular velocities are expressed in the hull coordinate system:

$$\boldsymbol{v} = (\boldsymbol{v}_1, \boldsymbol{v}_2) = (u, v, w, p, q, r) \quad (2)$$

Velocities in the geodetic and hull coordinate systems can be linked by the three angular motions (Euler angles) of the hull:

$$\begin{aligned} \boldsymbol{v}_1 &= \boldsymbol{J}_1^{-1} \cdot \dot{\boldsymbol{\eta}}_1, & \boldsymbol{v}_2 &= \boldsymbol{J}_2^{-1} \cdot \dot{\boldsymbol{\eta}}_2, \\ \dot{\boldsymbol{\eta}}_1 &= \boldsymbol{J}_1 \cdot \boldsymbol{v}_1, & \dot{\boldsymbol{\eta}}_2 &= \boldsymbol{J}_2 \cdot \boldsymbol{v}_2 \end{aligned} \quad (3)$$

where \boldsymbol{J}_1 and \boldsymbol{J}_2 are conversion matrices with the following expressions:

$$\boldsymbol{J}_1 = \begin{bmatrix} \cos \theta \cos \psi & \sin \phi \sin \theta \cos \psi - \cos \phi \sin \psi & \cos \phi \sin \theta \cos \psi + \sin \phi \sin \psi \\ \cos \theta \sin \psi & \sin \phi \sin \theta \sin \psi + \cos \phi \cos \psi & \cos \phi \sin \theta \sin \psi - \sin \phi \cos \psi \\ -\sin \theta & \sin \phi \cos \theta & \cos \phi \cos \theta \end{bmatrix} \quad (4)$$

$$\boldsymbol{J}_2 = \begin{bmatrix} 1 & \sin \phi \tan \theta & \cos \phi \tan \theta \\ 0 & \cos \phi & -\sin \phi \\ 0 & \frac{\sin \phi}{\cos \theta} & \frac{\cos \phi}{\cos \theta} \end{bmatrix} \quad (5)$$

Wave Model

The wave elevation can be represented as the sum of numerous small wavelets:

$$\eta(x, y, t) = \sum_n c_n \cos(k_n x \cos \theta_n + k_n y \sin \theta_n - \omega_n t + \varepsilon_n) \quad (6)$$

The surface elevation is normally distributed about a most probable value, η_d^* . And the surface elevation η can be described as a function of time, by:

$$\eta^*(\tau) = \alpha \rho(\tau) + g(\tau) \quad (7)$$

where $\tau = t - t_1$, α is the crest elevation and t_1 is the time when the waves focus. $\rho(\tau)$ is the autocorrelation function of the ocean surface elevation. $\alpha \rho(\tau)$ is the domestic component of crest elevation. $\rho(\tau)$ changes along with time as shown in Fig. 1:

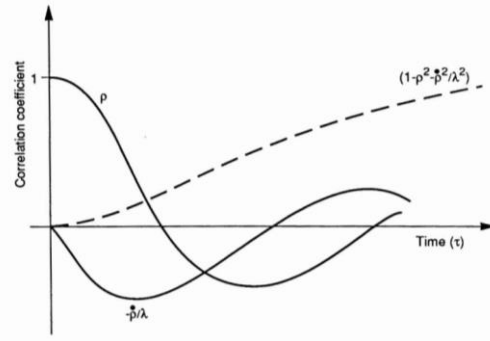


Fig. 1 The correlations of ρ and time

As τ increase, the conditioning imposed by the crest becomes weaker. The value of $\rho(\tau)$ is easily obtained as the Fourier transform of the surface spectrum.

$$\rho(\tau) = \frac{1}{\sigma^2} \int_0^\infty S(\omega) \cos \omega \tau d\omega = \frac{1}{\sigma^2} \sum_n (S(\omega) \Delta \omega_n) \cos \omega_n \tau \quad (8)$$

Thus the deterministic component of Eq.7 that will be dominant when α is large is

$$\eta_d^* = m = \frac{\alpha}{\sigma^2} \sum d_n \cos \omega_n \tau \quad (9)$$

where

$$d_n = S(\omega_n) \Delta \omega_n \quad (10)$$

Even when α is not large Eq.9 provides the expected and most probable values of the ocean surface displacement.

Simulation of Focused Waves

In order to reproduce the extreme waves numerically, the common means is to get a larger wave amplitude by adjusting the phase of the regular waves at different frequencies so that they reach the maximum amplitude at a certain moment and a certain position at the same time. Feng applied a phase-manipulation method to do an experiment on focused wave-current interaction. In this paper, focused waves are obtained based on linear and irregular wave theory, and the amplitude and frequency of each regular wave are obtained from the irregular wave wind and wave spectra.

The discretization of the linear wave parameters is accomplished based on the JONSWAP spectrum with the following spectral equation,

$$S(f) = 0.204 H_s^2 f_p^4 f^{-5} \left(-\frac{5}{4} \right) \exp \left(\left(\frac{f}{f_p} \right) \right) \gamma^r \quad (11)$$

$$r = \exp \left[\frac{-(f - f_p)^2}{2\sigma^2} f_p^2 \right] \quad (12)$$

where H_s is the meaningful wave height, $f_p = 1/T_p$ is the peak frequency, T_p is the peak period, γ is the peak lifting factor, which is generally taken as 3.3, and σ is the peak shape factor, which is defined as,

$$\sigma = \begin{cases} 0.09f \geq f_p \\ 0.07f < f_p \end{cases} \quad (13)$$

Focused waves are obtained in the form of a superposition of regular waves, and the wavefront equation $\eta(x, t)$ can be expressed as,

$$\eta(x, t) = \sum_{i=1}^N a_i \cos(k_i x - 2\pi f_i t + \varphi_i) \quad (14)$$

where i denotes the i^{th} linear wave, N is the total number of linear waves, a_i is the wave amplitude, k_i is the number of waves, f_i is the wave frequency, and the number of waves satisfies the dispersion relation with the wave frequency: $\omega_i^2 = (2\pi f_i)^2 = g k_i \tanh k_i h$, ω_i denotes the wave-circle frequency, g is the gravitational acceleration and h is the water depth.

NUMERICAL MODEL AND SIMULATION CONDITIONS

Geometric Model

The model selected in this paper is KCS Ship Model. The length between perpendiculars is 2.7m.

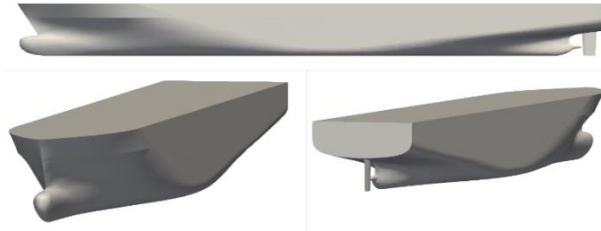


Fig. 2 Benchmark ship model KCS

Table 1 Main parameters of KCS

Parameters	Full scale	Model scale
L_{pp}	230m	2.7m
B	32.2m	0.378m
D	19m	0.223m
T	110.8m	0.084m
∇	52030m ³	0.084m ³

In the focused wave simulation, the distance from the focusing position to the inlet boundary should be long enough to ensure that the wave can be formed, and the specific computational domain size is set as: $-1.5L_{pp} < X < 3.5L_{pp}$, $-1.0L_{pp} < Y < 1.0L_{pp}$, $-2.0L_{pp} < Z < 1.0L_{pp}$.

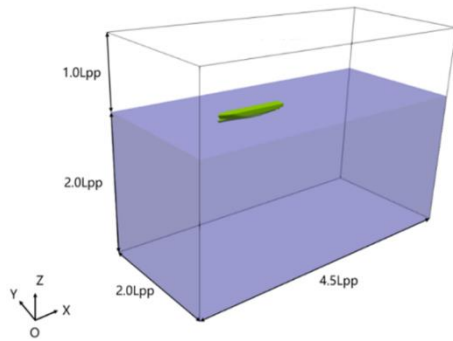


Fig. 3 Computational domain

A wave-making relaxation region of $0.5L_{pp}$ in length is provided at the inlet of the computational domain, and an extinction relaxation region of $1.0L_{pp}$ in length is provided at the outlet.



Fig. 4 Demonstration of relaxation zone

Computational Grids

Overlapping mesh is used to avoid the large mesh deformation caused by the large hull movement, which results in low mesh quality. Encryption is performed around the hull and at the waterline surface to capture the details of the flow field. At least 20 grids are guaranteed for a wave height in the z-direction and 200 grids are guaranteed for a wavelength in the x-direction.

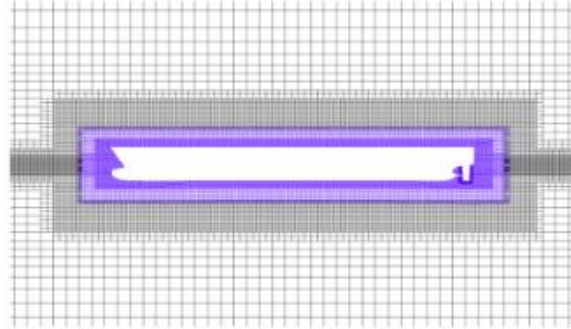


Fig. 5 Grid arrangement

Simulation Conditions

The wave spectrum is JONSWAP. There are two amplitude and two periodicities.

Table 2. Main parameters of focused wave

Parameters	Case A	Case B	Case C
Amplitude	0.108m	0.108m	0.054m
T_p	3.72s	1.86s	1.86s
Focus time	t=10s		

the peak of the focused wave is set to be focused at the bow, and the pressure distributions of the ship are compared on the bow.

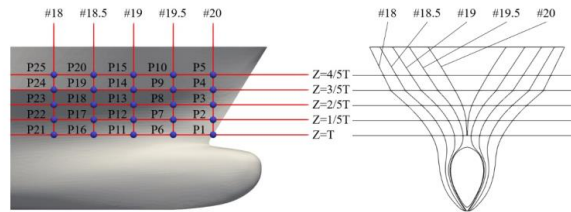


Fig. 6 Position of probes

RESULT AND DISCUSSION

Wave Validation

The time history of wave at the focusing position is shown in Fig.6. Three different amplitudes of waves are used to be compared with theory. It can be seen that the numerical solution agrees well with the theoretical solution for a period of time before the generation of the focused wave, and deviations start to appear on the waveforms before and after the moment of focusing, and this deviation becomes more obvious as the amplitude of the focused wave increases. This phenomenon may be due

to the greater wave steepness of the maximum wave peak and the enhanced interference between the sub-waves, which in turn causes the wave to become unstable near the focused wave moment. After the passage of the maximum wave peak, the numerical solution again agrees well with the theoretical solution.

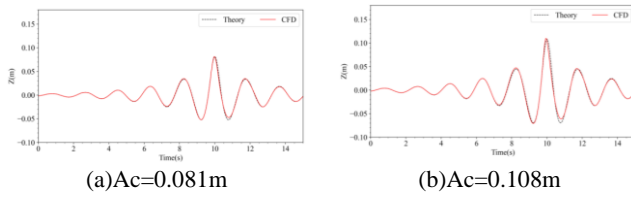


Fig. 7 Comparison of wave elevation between theory and CFD

Overall, although the numerical solution deviates from the theoretical solution, the error of the maximum wave amplitude is not more than 2%, the error of the focusing moment is not more than 1%, and the main features of the focused wave are preserved, which indicates that the current numerical method can simulate the focused wave more accurately, and this provides support for the subsequent research under the focused wave.

Results

Extracting the ship's motion attitude and mapping the hull surface pressure when the wave is focused. And p_rgh refers to dynamic pressure obtained by subtracting hydrostatic pressure from hull surface pressure.

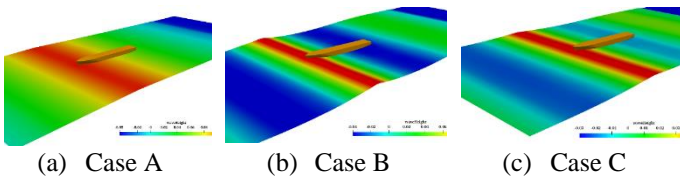


Fig. 8 Wave elevation

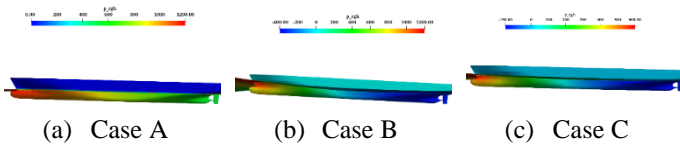


Fig. 9 Pressure distribution along ship

Comparing Fig.8(a) and Fig.8(c), we could find though they have the same amplitude, a shorter wavelength result in a higher wave steepness, making the ship's motion more violent. Comparing Fig. 9(a) with Figs. 9(b) and Fig. 9(c), it can be seen that although the maximum value of the dynamic pressure on the hull surface at the moment of wave focusing occurs at the bow under different conditions, the location of the minimum value of the dynamic pressure varies under different conditions. The dynamic pressure of the hull above the free surface is always 0, and the dynamic pressure of the stern part of the hull is negative for both cases B-C, while the dynamic pressure of the transom part of the hull is still positive for case A. This may be due to the fact that the longer wavelength makes the wave steepness more gentle at the moment of wave focusing, and by the time the peak of the focused wave has progressed to the bow of the ship, the trough of the previous wave has progressed aft of the stern, and the entire hull of the ship is on the currently focused wave. At shorter wavelengths, when the wave is focusing at the bow, the trough of the previous wave has already

developed near the stern, which reduces the pressure of wave action on the stern part of the ship, and the ship's stern shows a negative dynamic pressure.

Extract the data from the measurement point Probe95 for comparison.

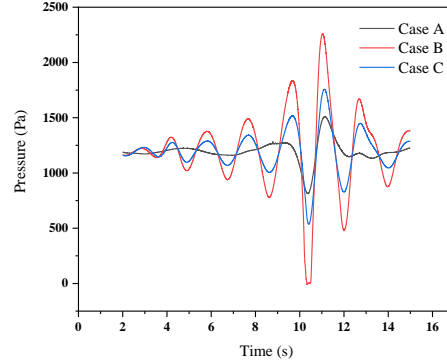


Fig. 10 Time history of total pressure

Observing Fig. 10, it can be found that the total pressures at the moment of wave focusing are, in descending order, case B, C and A. Although case A has twice the amplitude of the wave height of case C, the maximum value of the total pressure of case C is higher than that of case A. The maximum value of the total pressure of case C is higher than that of case A, even though case A has twice the amplitude of the wave height. Meanwhile, the total pressure time histories of cases B and C were in good agreement with the wave time histories, while the pressure time histories of case A did not match the wave time histories for the overall changes outside the wave focusing moment. Take the same pressure point and compare the dynamic pressure.

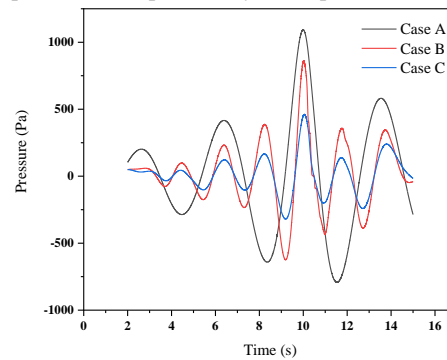


Fig. 11 Time history of dynamic pressure

Unlike the total pressure, the dynamic pressure maximum for case A is higher than that for cases B and C. Also, the dynamic pressure time history for case A agrees well with the wave time history.

Table 3. Maximum value of pressure and time of occurrence

	Case A	Case B	Case C
p	1509.5Pa	2262.2Pa	1757.3Pa
Time	11.15s	11.03s	11.10s
p_rgh	1093.7Pa	862.21Pa	461.58Pa
Time	9.99s	10.02s	10.06s

Table 3 and comparison of Fig.10 and Fig. 11 reveals that the total pressure change has a hysteresis compared to the wave time calendar, while the dynamic pressure change is able to respond quickly with the

wave change. Meanwhile, comparing the pressure time histories of case A, it can be found that the total pressure has no obvious peaks and valleys before and after the wave focus, while the dynamic pressure shows obvious peaks and valleys; and the total and dynamic pressures of case B and C show obvious peaks and valleys.

This suggests that the free surface of case A may have echoes resulting in a gap between the actual wave generation and the theory. Higher wavelengths with the same length of the dissipative relaxation zone result in lower wave generation quality. The distribution of the pressure in the frequency domain is obtained by applying the Fourier transform to the pressure time history.

By comparing the distributions of the pressure in the frequency domain for case A, B and C, it can be found that the pressure for case B and C is mainly dominated by waves with frequencies around 0.4-0.6 Hz, and the overall shape shows a single peak. However, for case A, the frequency domain distribution of dynamic pressure is similar to that of case B and C, showing a single peak, but the total pressure does not show an obvious spike, which further proves that a longer wavelength with the same length of the relaxation zone will lead to a decrease in the quality of wave dissipation and thus cause echoes, which will have an effect on the generation of subsequent waves. At the same time the amplitude of the total pressure is significantly lower than that of the dynamic pressure case; whereas the peak amplitude of the single peak is similar for working cases B and C.

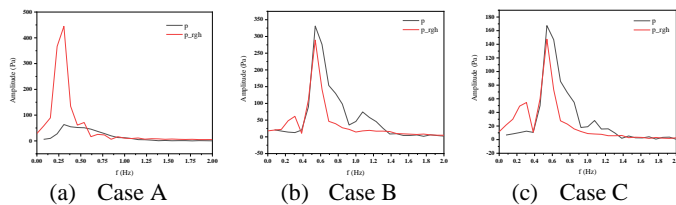


Fig. 12 Distribution of pressure in frequency domain

ACKNOWLEDGEMENT

This work is supported by the National Natural Science Foundation of China (52131102), to which the authors are most grateful.

REFERENCE

Chen, ST, Zhao, WW, and Wan, DC (2022). "On the scattering of focused wave by a finite surface-piercing circular cylinder: A numerical investigation." *Phys. Fluids*, 34(3), 035132.
 Feng, X, Taylor, PH and Dai, S (2020). "Experimental investigation of higher harmonic wave loads and moments on a vertical cylinder by a phase-manipulation method." *Coast. Eng.*, 160, 103747.

CONCLUSION

This paper focuses on calculating the response of a KCS ship model in focused waves using a combination of overset grids from SUGGAR++ and OpenFOAM and the third-party wave-making software waves2FOAM, and comparing the total and dynamic pressures for different operating cases.

At shorter wavelengths, a region of negative dynamic pressure occurs below the free surface of the stern at the moment of wave focusing, which may be due to the higher wave steepness in the short-wavelength condition and the fact that the transom is in the trough of the previous wave when the wave focuses at the bow, resulting in a negative dynamic pressure at the stern.

At the same length of the relaxation zone, longer wavelengths lead to a degradation of the quality of the extinction, and the presence of echoes causes the wave height lift to diverge from the theoretical value, having an effect on the time-calendar variation of the total pressure, while having almost no effect on the variation of the dynamic pressure. The distribution of the pressure in the frequency domain shows an overall single-peak pattern, but for the longer wavelength case, the dissipation quality decreases with the same length of the relaxation region, so that the frequency domain distribution of the total pressure does not show an obvious spike, while the amplitude is significantly lower than that of the short wavelength case.

Fonseca, N, Carlos GS, and Ricardo, P (2005). "Global loads on an FPSO induced by a set of freak waves." *Proc 15th Int Offshore and Polar Eng Conf*, Seoul, ISOPE, 41960, 647-654.
 Liu, D, Li, F, and Liang, L (2022). "Numerical study on green water and slamming loads of ship advancing in freak wave." *Ocean Eng.*, 261, 111768, 47-64.
 Liu, Z, Zhuang, Y, and Wan, DC (2020). "Numerical Study of Focused Wave Interactions with a Single-Point Moored Hemispherical-Bottomed Buoy." *Proc 30th Int Ocean and Polar Eng Conf*, Shanghai, ISOPE, 30(01), 53-61.
 Perić, R, Vukčević, V, Abdel-Maksoud, M, and Jasak, H (2022). "Optimizing wave generation and wave damping in 3D-flow simulations with implicit relaxation zones." *Coast. Eng.*, 171, 104035, 87-102.
 Stansberg, CT, and Karlsen, SI (2001). "Green sea and water impact on FPSO in steep random waves." *17th Practical Design of Ships and Other Floating Structures*, Shanghai, PRADS, Elsevier Science Ltd, 1, 593-601.
 Tromans, Peter S, Ali R, Anaturk and Paul H (1991). "A new model for the kinematics of large ocean waves-application as a design wave." *Proc 1st Int Offshore and Polar Eng Conf*, Edinburgh, ISOPE, 3, 64-71.
 Zhuang, Y, Zhou, FC, Zhou, WJ, and Wan, DC (2023). "Numerical investigations of focused wave interact with a moving cylinder." *J. Hydrodyn*, 35(4), 724-735.